

See discussions, stats, and author profiles for this publication at: <https://www.researchgate.net/publication/258255698>

# Effect of Click-Chemistry Approaches for Graphene Modification on the Electrical, Thermal, and Mechanical Properties of Polyethylene/Graphene Nanocomposites

ARTICLE *in* MACROMOLECULES · NOVEMBER 2013

Impact Factor: 5.8 · DOI: 10.1021/ma401606d

---

CITATIONS

18

---

READS

158

## 5 AUTHORS, INCLUDING:



Marta Castelaín

Spanish National Research Council

11 PUBLICATIONS 98 CITATIONS

[SEE PROFILE](#)



Gary Ellis

Spanish National Research Council

127 PUBLICATIONS 1,964 CITATIONS

[SEE PROFILE](#)



Horacio Salavagione

Instituto de Ciencia y Tecnología de Polímeros

65 PUBLICATIONS 1,361 CITATIONS

[SEE PROFILE](#)

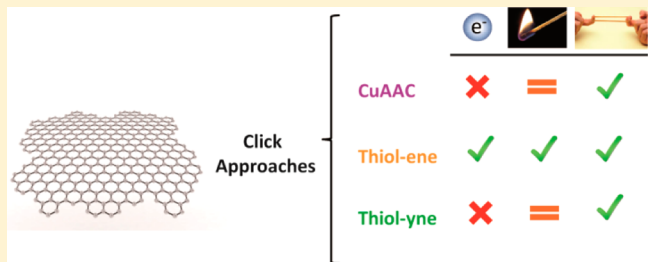
## Effect of Click-Chemistry Approaches for Graphene Modification on the Electrical, Thermal, and Mechanical Properties of Polyethylene/Graphene Nanocomposites

Marta Castelaín, Gerardo Martínez, Carlos Marco, Gary Ellis, and Horacio J. Salavagione\*

Departamento de Física de Polímeros, Elastómeros y Aplicaciones Energéticas, Instituto de Ciencia y Tecnología de Polímeros, CSIC, c/Juan de la Cierva, 3, 28006 Madrid, Spain

### Supporting Information

**ABSTRACT:** The effect of the type of chemical route used to functionalize graphene with short-chain polyethylene on the final properties of graphene-based high density polyethylene nanocomposites is reported. Three different click reactions, namely copper-catalyzed alkyne–azide (CuAAC), thiol–ene and thiol–yne have been addressed. The nanocomposites were prepared using a method that we denote “gradient interphase”. The electrical and thermal conductivity and the mechanical properties strongly depend on the click reaction used to modify graphene, the thiol–ene reaction giving the best results. This study demonstrates that the election of the chemical strategy to provide graphene with functionalities common to the polymer matrix and the engineering of the interface are crucial to obtain nanocomposites with improved properties.



### INTRODUCTION

Graphene is considered by many as one of the next-generation nanofillers for polymer nanocomposites (PNCs) due to its unique properties and chemical functionalization capabilities.<sup>1–7</sup> Its use as a reinforcement in a polymer matrix may significantly alter structure–property features of polymers without sacrificing processability nor adding excessive weight. In such materials, precise interfacial control and dispersion of the filler in the polymer hosts are crucial aspects for properties design. Nevertheless, due to its strong tendency for van der Waals interactions and high specific surface area, graphene layers tends to aggregate in an almost irreversible manner making effective dispersion in the polymeric matrix very difficult.<sup>4,8,9</sup> Thus, the key to achieve good dispersion consists in furnishing graphene with adequate chemical functionality that is able to effectively interact with the polymer host leading to stronger interfaces.

This strategy first focused on the functionalization of graphene with small, single molecules,<sup>10–18</sup> but over the past 4–5 years, the direct functionalization of graphene with polymers has been demonstrated as an interesting alternative.<sup>4,6,8,19–25</sup> The direct coupling of graphene with preformed relatively high molecular weight polymers generally has low yield because of the large steric hindrance associated with connecting a polymeric entity with a graphene particle.<sup>6,21</sup> However, modification with low-molecular weight polymers or oligomers and the posterior use of this polymer-modified graphene as a filler for high molecular weight polymers emerges as a powerful strategy whereby the low-molecular weight polymer brushes emerging from the graphene sheet may be expected to adopt the role of a vehicle to improve the

graphene/polymer interface. In this case the chemical reaction chosen to modify the graphene can directly affect the final properties of the material.

First demonstrated for the coupling of simple molecules, click chemistry reactions have been successfully extended to the field of polymers<sup>26</sup> and more recently to carbon nanostructures including carbon nanotubes<sup>27</sup> and graphene.<sup>6,24,25,28–32</sup> The principal characteristics of click reactions are, among others, that they are wide in scope and easy to perform, use only readily available reagents, and are insensitive to oxygen and water.<sup>33–36</sup> In particular, of this type of reaction the copper catalyzed azide–alkyne cycloaddition (CuAAC)<sup>6,24,25,30,31</sup> has been the most employed for the modification of graphene.<sup>6,24,25,30,31</sup> On the other hand, while other click strategies such as thiol–radical approaches (thiol–ene and thiol–yne) have been widely used with polymers,<sup>36–52</sup> these are in their early stages of implementation with graphene, and the initial results look highly promising.<sup>53</sup>

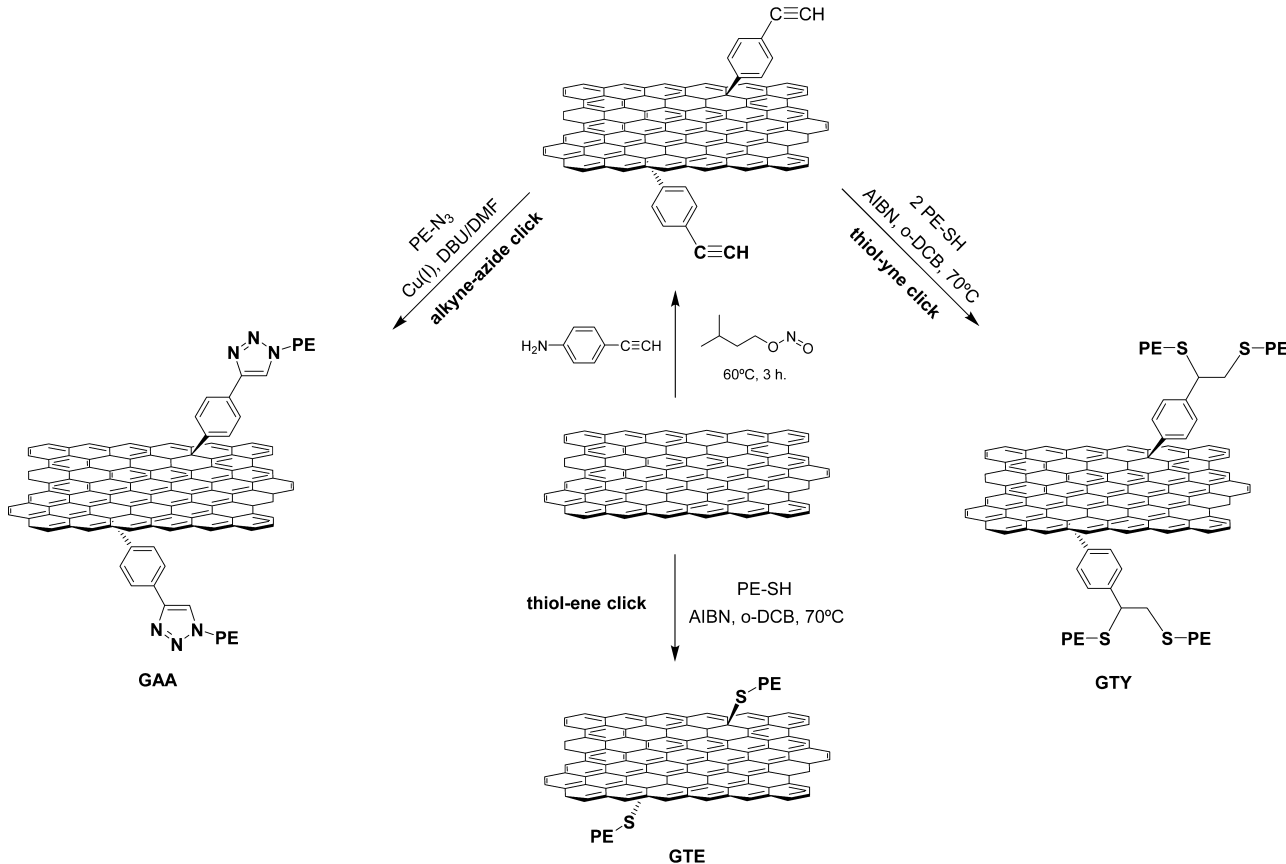
This work studies the functionalization of graphene with brushes of short-chain polyethylene (PE) using three different click approaches including CuAAC, thiol–ene and thiol–yne reactions, and analyzes the effect of the chemistry used on the final properties of nanocomposites of PE-modified graphene with high density polyethylene (HDPE). It is observed that mechanical properties as well as thermal and electrical conductivity of the nanocomposites strongly depend on the synthetic procedure used to modify graphene. As all the

Received: July 31, 2013

Revised: October 22, 2013

Published: November 5, 2013

Scheme 1. Grafting PE Brushes to the Graphene Surface by CuACC, Thiol–Ene and Thiol–Yne Reactions



nanocomposites were prepared under the same protocol the reasons to explain this dependency are found in the graphene source (that is not the same in all cases), the grafting density of PE brushes, etc.

## EXPERIMENTAL SECTION

**Materials.** Graphene (Angstrom Materials), Polyethylene monoalcohol (PE-OH,  $M_n = 460 \text{ g}\cdot\text{mol}^{-1}$ , Aldrich), carbon tetrabromide (Aldrich), copper(I) iodide (CuI, Aldrich  $\geq 99.5\%$ ), 1,8-Diazabicyclo[5.4.0]undec-7-ene (DBU, Aldrich, 98%), sodium hydrogenosulfide (NaSH, Aldrich), 2,2'-azobis(2-methylpropionitrile) (AIBN, Aldrich), toluene (Merck), methanol (Sigma), tetrahydrofuran (THF, Aldrich), dichloromethane ( $\text{Cl}_2\text{CH}_2$ , Aldrich) and *o*-dichlorobenzene (*o*-DCB, Aldrich) were used as received without further treatment. A commercial high density polyethylene (HDPE, MFI = 0.15 dL per 10 min (2.16 kg), density = 945  $\text{kg}\cdot\text{m}^{-3}$ ) was kindly supplied by Repsol, Spain.

**Preparation of PE-Brushes Clicked to Graphene.** The approaches addressed to click graphene with PE are illustrated in Scheme 1.

**Approach 1. CuAAC.** This reaction involves coupling between an alkyne group and an azide moiety that are provided by the graphene and the polymer, respectively. The graphene was furnished with alkyne groups by following a previously reported procedure,<sup>29</sup> while the azide-terminated polymer was prepared by bromination of PE-OH and subsequent nucleophilic attack with sodium azide (see electronic Supporting Information for more details). For the click reaction alkyne functionalized graphene (200 mg) and DMF (75 mL) were placed into a 100 mL flask. The mixture was sonicated until a good suspension was achieved, and then azide-functionalized polyethylene (232 mg, 0.50 mmol), CuI (190 mg, 1.00 mmol) and DBU (7.6 g, 50.00 mmol) were added. The reaction was conducted under nitrogen atmosphere at 60 °C for 24 h. After cooling to room temperature, the

mixture was diluted with 200 mL of THF, bath sonicated for 5 min and filtered through a 200 nm PTFE membrane. The product was washed thoroughly with THF (5 × 100 mL), methanol, aqueous ammonium hydroxide solution (28%), water, methanol, and  $\text{CH}_2\text{Cl}_2$  (1 × 100 mL of each), and then dried under vacuum overnight. The product was denominated GAA.

**Approach 2. Thiol–Ene.** This procedure uses pristine graphene as a hyper-conjugated alkene and a thiol-terminated PE (synthetic details for PE-SH given in the Supporting Information). For the click reaction 0.5 g of PE-SH was dissolved in 50 mL of anhydrous *o*-DCB, under nitrogen atmosphere. Then, a thermal-initiator (AIBN 1.72 g, 0.01 mol) and graphene (0.5 g) were added to the polymer solution. The mixture was heated at 70 °C and stirred overnight. The solid product was collected by filtration and washed with abundant amounts of methanol and hot toluene to remove excess initiator and nonreacted polymer, respectively. Soxhlet extraction in hot toluene was also conducted in order to remove free polymer, but no differences were observed after the extraction. The product was denominated GTE.

**Approach 3. Thiol–Yne.** This procedure used the same polymer as in approach 2 and the alkyne-modified graphene employed in approach 1. For the click coupling the AIBN initiator (1.72 g, 0.01 mol) and the alkyne-modified graphene (0.25 g) were added to a solution of PE-SH (0.5 g) in 50 mL of anhydrous *o*-DCB under nitrogen atmosphere. The mixture was heated to 70 °C and left overnight. The solid product was collected by filtration and thoroughly washed with methanol and hot toluene to remove excess initiator and nonreacted polymer, respectively. The product was denominated GTY.

**Preparation of Graphene/HDPE Nanocomposites.** Nanocomposites of HDPE with GAA, GTE, and GTY were prepared using the same protocol. A nanocomposite of HDPE and the starting pristine graphene (without any chemical treatment) was also prepared under the same protocol and used as a control. The nanocomposites were prepared as follows: 200 mg of the graphene (G) or modified

graphene (GAA, GTE or GTY) were mixed with 200 mg of PE-OH in 20 mL of warm xylene (90 °C) under vigorous stirring. Subsequently the mixtures were precipitated in methanol, filtered, washed with methanol and thoroughly dried under vacuum. Samples were denominated GAA/PE-OH, GTE/PE-OH, and GTY/PE-OH, respectively. These mixtures with a graphene/polymer composition of around 50/50 were subsequently used as a filler for nanocomposites with HDPE. For this purpose all fillers were mixed with HDPE in xylene in order to obtain nanocomposites with final filler content of ca. 1%. The mixtures were then precipitated with methanol, and dried under vacuum. Samples were denominated G-HDPE, GAA-HDPE, GTE-HDPE and GTY-HDPE. Finally, hot-pressed films of all nanocomposites were prepared at 140 °C and a pressure of 100 bar and these were used to study the properties outlined below.

**Characterization.** All clicked products were characterized by vibrational spectroscopy. IR spectra were recorded on a Perkin–Elmer System 2000 FTIR spectrometer. The samples were mixed with KBr and compressed pellets were prepared for analysis in the spectral range of 4000–500 cm<sup>-1</sup> at a resolution of 4 cm<sup>-1</sup>. Raman measurements were made in the Raman Microspectroscopy Laboratory of the Characterization Service in the Institute of Polymer Science & Technology, CSIC. A Renishaw InVia Reflex Raman system (Renishaw plc, Wotton-under-Edge, U.K.) was used employing a grating spectrometer with a Peltier-cooled charge-coupled device (CCD) detector, coupled to a confocal microscope. All spectra were processed using Renishaw WiRE 3.2 software. The Raman scattering was excited using an argon ion laser wavelength of 514.5 nm. The laser beam was focused on the sample with a 100 microscope objective (N.A. = 0.90), with a laser power at the sample of around 2 mW.

Thermogravimetric analysis was carried out using a TA Instruments Q50 thermobalance between 50–800 °C at a heating rate of 10 °C min<sup>-1</sup>, under an inert atmosphere (nitrogen, 60 cm<sup>3</sup> min<sup>-1</sup>). Samples were analyzed using TA Instruments Universal Analysis 2000 software (version 4.5A, Build 4.5.0.5). For isothermal scans, the samples were heated at a scan rate of 10 °C min<sup>-1</sup> from room temperature to 650 °C and maintained at that temperature during 8 h, or until constant weight was reached.

The crystallization and melting behavior were investigated by differential scanning calorimetry (DSC) employing a Mettler TA4000/DSC30 equipment with STARe software. The experiments were carried out under nitrogen using samples of ~6 mg sealed in aluminum pans. These were heated from 0 to 160 °C, maintained at this temperature for 5 min, then cooled to 0 °C and heated again to 160 °C. Heating and cooling rates of 10 °C min<sup>-1</sup> were used in all cases. The transition temperatures were taken as the peak maxima/minima in the calorimetric curves.

The dispersion of the nanofillers in the HDPE matrix was examined by scanning electron microscopy (SEM) by using a SU8000 Hitachi scanning electron microscope in the Characterization Service of the Institute of Polymer Science & Technology. The nanocomposite samples were cryofractured from film hot-pressed films and subsequently coated with ca. 5 nm Au/Pd overlayer to avoid charging during electron irradiation.

The thermal conductivity ( $k$ ) was calculated from eq 1

$$k = \rho C_p \alpha \quad (1)$$

where  $\rho$  is the density of the materials,  $C_p$  is the specific heat and  $\alpha$  is the thermal diffusivity.

Room temperature thermal diffusivity measurements, based on the pulsed-laser method, were performed with a ThermoFlash 2200 (Holometrix Inc.). In this method one side of the sample (~0.3 to 0.5 mm thick) is heated by a laser pulse (1060 nm, power of 15 J), the heat absorbed at the surface is transmitted through the sample and produces a temperature rise on the opposite side. This increase is reflected as a function of time by an infrared detector (InSb). The reported values correspond to the average of at least three specimens.

The experimental value of specific heat capacity ( $C_p$ ) was determined by DSC using a standard reference of Al<sub>2</sub>O<sub>3</sub> (M-29595). Three cycles of heating/cooling between 0 and 50 °C at 5 °C

min<sup>-1</sup> were applied to verify data reproducibility. Prior to the heating scans the samples were heated from room temperature to 160 °C, then held at 160 °C for 1 min, cooled from 160 to 0 °C and held at the latter for 1 min. Five specimens of each sample were used and the experimental value of  $C_p$  was taken as the average value discarding the highest and lowest values.

DC-conductivity measurements were carried out on pellets or films perfectly dried under vacuum 24h. The measurements were made using a four-probe setup equipped with a dc low-current source (LCS-02) and a digital microvoltmeter (DMV-001) from Scientific Equipment & Services. The conductivity was calculated by the following equation:

$$\sigma = \frac{1}{\rho} = 4.5234t \left( \frac{V}{I} \right) f_1 f_2 \quad (2)$$

Here  $t$  is the thickness of the sample,  $f_1$  is the finite thickness correction for thick samples on an insulating bottom boundary, and  $f_2$  is the finite width correction.

Tensile properties of the composites were measured with an Instron 4204 tensile tester at room temperature and 50 ± 5% relative humidity, using a crosshead speed of 10 mm min<sup>-1</sup> and a load cell of 100 N. Five specimens for each type of composite were tested to ensure reproducibility.

## RESULTS AND DISCUSSION

The different approaches to furnish graphene with short-chain PE brushes are shown in Scheme 1 where it can be seen that while the thiol–ene reaction proceeds directly on the graphene surface, the other two click reactions need previous modification of the graphene surface with alkyne moieties. Independent of the graphene source or reaction conditions, the click modifications proceeded reasonably well in all cases, and PE brushes were successfully grafted to the carbonaceous surface. Although the samples produced are black or dark brown powders because of the high graphene content, the infrared spectra of GAA, GTE and GTY clicked products clearly showed the characteristic PE bands (Figure 1A). The GTY sample clearly shows all the characteristic vibrations of PE including the doublets at 1472/1463 cm<sup>-1</sup> (–CH<sub>2</sub> bending) and 730/718 cm<sup>-1</sup> (–CH<sub>2</sub> rocking) and the C–H symmetric and antisymmetric stretching of –CH<sub>2</sub> groups, at 2922 and 2849 cm<sup>-1</sup>, respectively. In the case of GTE and GAA samples

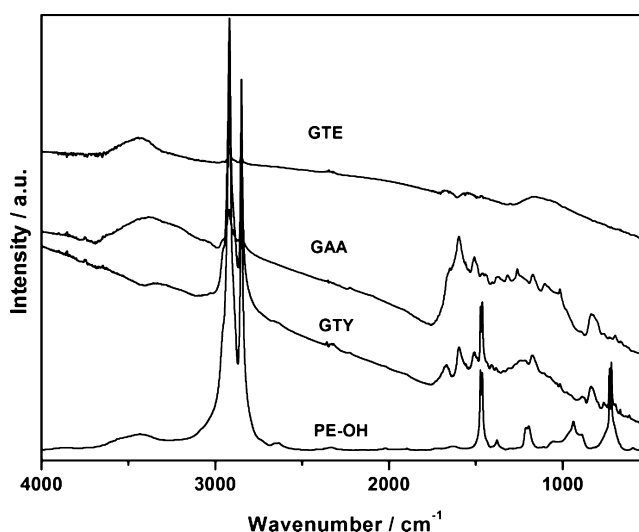


**Figure 1.** FTIR transmission spectra of the PE-OH starting material and the clicked products.

only the most intense PE bands associated with the C–H stretches could be detected. Further, in the case of the samples GTY and GAA the FTIR spectra show several additional bands at 1660, 1598, 1506, and 830  $\text{cm}^{-1}$  that arise from the aromatic groups of alkyne-modified graphene (Figure 1).

The differences in the intensity of the PE bands in the products can be attributed to differences in the final graphene/PE ratio obtained via the different synthetic routes. In the case of GTY it is worth mentioning that the thiol–yne reaction allows the introduction of two polymer chains per functional alkyne group giving a double-branched modification that is expected to increase the final concentration of the polymer. On the contrary, the fact that the thiol–ene reaction must occur on the neat graphene surface makes the reactivity quite low as it is sterically hindered.<sup>36,40</sup> Finally, the case of GAA is intermediate between the other two, because the reaction does not occur directly on the graphene surface but only allows the introduction of one PE arm per alkyne moiety on graphene.

In order to estimate the grafting density for each sample, TGA measurements were conducted (Figure 2). From the plots

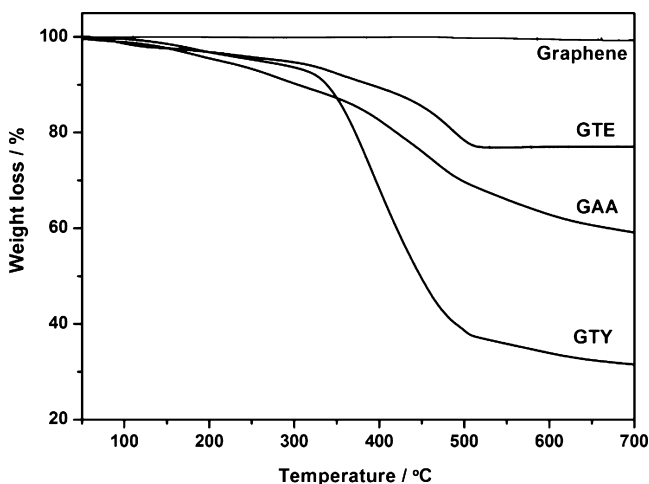


Figure 2. TGA curves of graphene and its clicked products heated at 10  $^{\circ}\text{C}\cdot\text{min}^{-1}$  under N2 atm.

obtained a very different behavior can be observed as a function of the chemical modification procedure, with a mass loss at 700  $^{\circ}\text{C}$  of 18, 38 and 64% for GTE, GAA and GTY, respectively. Since in the dynamic thermograms the weight did not reach constant values (especially samples GTY and GAA), isothermal TGA at 650  $^{\circ}\text{C}$  were conducted (Figure S2, Supporting Information) to verify the mass losses values, obtaining 23, 41 and 70% for GTE, GAA and GTY, respectively. Although the values observed were slightly higher than those obtained by dynamic scans, the variation as a function of the type of chemical route used remains. These results clearly indicate that the largest degree of functionalization was obtained for the GTY. This is logical, since the thiol–yne click reaction allows the incorporation of two polymer chains per alkyne group. With the data obtained from the TGA curves we can roughly estimate the grafting density achieved for each reaction. In the case of GTE, the calculation is simple as the PE is conducted directly onto the graphene surface, and a grafting density of 1 PE brush per 180 carbon atoms was obtained. For the other two samples (GAA and GTY), since the reaction is conducted on the alkyne modifying groups we must consider other aspects, i.e. the grafting density on alkyne-modified graphene

and the site where the bond scission occurs resulting in the elimination of the modifying PE brushes. For the former, we have previously determined by TGA that alkyne-modified graphene has a mass loss of around 20 wt % (2.5 mmol per gram).<sup>54</sup> Using the data from TGA, the molar mass of carbon (12 g·mol<sup>-1</sup>) and the modifying group (92 g·mol<sup>-1</sup>) and following the methods reported by Ye et al.<sup>6</sup> we can estimate that the mass loss corresponds to the incorporation of approximately one functional group per 34 carbon atoms. So, it is reasonable to assume that we have a sufficiently high concentration of alkyne groups available to react with the PE chains. For the latter, from the TGA measurements we can accept that the modifying groups are removed in a single process, and assume that this represents bond scission at the carbon directly bound to the graphene surface; otherwise the TGA curves should clearly show more than one process. Thus, in the case of GAA, we observe that PE constitutes 75% of the mass of the evolved species (the other 25% comes from the benzene and triazole ring connecting graphene and PE, see Scheme 1), which corresponds to 0.64–0.67 mmol of grafted PE. Since one mole of PE reacts with one mole of alkyne we can estimate that approximately one in three alkyne groups has been clicked to a PE chain (fraction of reacted alkyne =0.32–0.37). In the case of GTY, PE accounts for 90% of the total mass loss (Scheme 1). This is equivalent to 1.31–1.37 mmol. In this reaction one alkyne group reacts with two PE chains and the fraction of clicked alkyne groups is almost identical to the value obtained in the previous case (ca. 0.33–0.36). However, the amount of polymer is much higher because one functional alkyne group reacts with two polymer chains.

The products were also characterized by Raman spectroscopy (Figure S3). Pristine graphene showed the typical D (1348  $\text{cm}^{-1}$ ), G (1589  $\text{cm}^{-1}$ ), 2D (2697  $\text{cm}^{-1}$ ) and D + G bands (2938  $\text{cm}^{-1}$ ). The D/G areas ratio, which is directly related to the quality of the  $\text{sp}^2$  network in graphene,<sup>18,55–57</sup> is quite high, typical of a defective material. Thus, the starting graphene can be considered as nanographene (fwhm =112)<sup>58</sup> with a high edge contribution, which can be the preferred points for radical attack. After modification the D/G ratio changed only slightly, but the full with half-maximum (fwhm) of the D band increased markedly (Figure S3c,d). These findings suggest that the C–C bond character is similar to that in the starting graphene, while the increased disorder implicit in the increase in fwhm(D) may arise from strain generated by linking of the polymer chains.<sup>59,60</sup>

With regard to the electrical properties of the clicked products, the electrical conductivity of the GTE sample was observed to be relatively high. This is in agreement with Raman results that suggest that the concentration of defects did not increase significantly after the modification. A conductivity value of 12.6  $\text{S}\cdot\text{cm}^{-1}$  was found that is roughly half the value of the starting graphene material (Table 1). In the case of the samples starting from alkyne-modified graphene (ALK-graphene) the conductivity values are much lower due to the low initial value for the starting material ( $6.3 \times 10^{-4} \text{ S}\cdot\text{cm}^{-1}$ ), and were found to be  $1.52 \times 10^{-4} \text{ S}\cdot\text{cm}^{-1}$  for GTY and  $3.35 \times 10^{-4} \text{ S}\cdot\text{cm}^{-1}$  for GAA. The lower value of the former may indeed be due to the greater amount of polymer coating the graphene sheet that would prevent further electron hopping between sheets. However, it can also originate from direct attack of the thiol radical on the graphene network creating some additional defects, but this mechanism has lower probability because of the low intrinsic reactivity of conjugated

**Table 1.** Variation of the Electrical Conductivity of the Different Modified Graphene Systems, Their Blends with PE-OH, and Nanocomposites with HDPE

sample	dc conductivity/S·cm <sup>-1</sup>
Starting Graphene and Derivatives	
graphene	~25
ALK-graphene	6.3 × 10 <sup>-4</sup>
GAA	3.35 × 10 <sup>-4</sup>
GTE	12.6
GTY	1.52 × 10 <sup>-4</sup>
After 1st Mixing Step with PE-OH	
GAA/PE-OH	~1 × 10 <sup>-4</sup>
GTE/PE-OH	9.6
GTY/PE-OH	not detected
Nanocomposites with HDPE with 1% of Filler	
G-HDPE	insulating
GAA-HDPE	insulating
GTE-/HDPE	~1 × 10 <sup>-7</sup>
GTY-/HDPE	insulating

alkenes<sup>35</sup> (in this case further decreased by steric hindrance). In fact, the Raman results suffice to discard this possibility (Figure S3b). Notwithstanding, the values lie in the same order of magnitude and are clearly limited by the quality of the initial graphene network.

**Properties of the Different Graphene-Based HDPE Nanocomposites.** Nanocomposites were prepared as detailed in the Experimental Section based on a protocol that can be defined as a “gradient interface”, where the short-chain polymer acts as compatibilizer between the HDPE and graphene. This strategy was implemented after initial attempts of direct mixing

of the modified graphenes with HDPE resulted in no change in the properties tested. Since the procedure is based on two steps consisting of dissolution–precipitation that can lead to loss of material, the final composition of the nanocomposites was determined by TGA from the remaining mass at 650 °C, a temperature at which the polymeric materials are completely eliminated (see Supporting Information, Figure S4).

In order to determine the degree of exfoliation of graphene as well as the quality of the nanofiller dispersion in the HDPE matrix, SEM was employed. Figure 3 shows the SEM images of the fracture surface of samples containing 1 wt % of the PE-OH/graphene filler, where a nanocomposite of HDPE with nonfunctionalized graphene prepared under identical conditions is also shown for comparison. This reference sample, G-HDPE was found to be somewhat heterogeneous with regions composed of pure polymer (demarcated with white lines) along with regions where the graphene appears to be better dispersed, and regions with aggregates (black line). In the samples using functionalized graphene the results are very different. While samples employing GTY and GAA show large graphene aggregates (indicated with arrows), in the GTE-HDPE sample (Figure 3D) the graphene laminates appear to be perfectly dispersed in the polymer matrix throughout the sampled area.

It is widely accepted that processing and dispersion of graphene in polymeric hosts constitutes the main challenge to its use in nanocomposites, the control of the interfacial interactions being crucial. This is the reason we employed three different chemical approaches to improve the graphene/HDPE interface. However, the results seem to be the opposite of those expected, since the samples with the poorest dispersion are those where the concentration of PE brushes on graphene is higher. We expected that the higher the degree of graphene

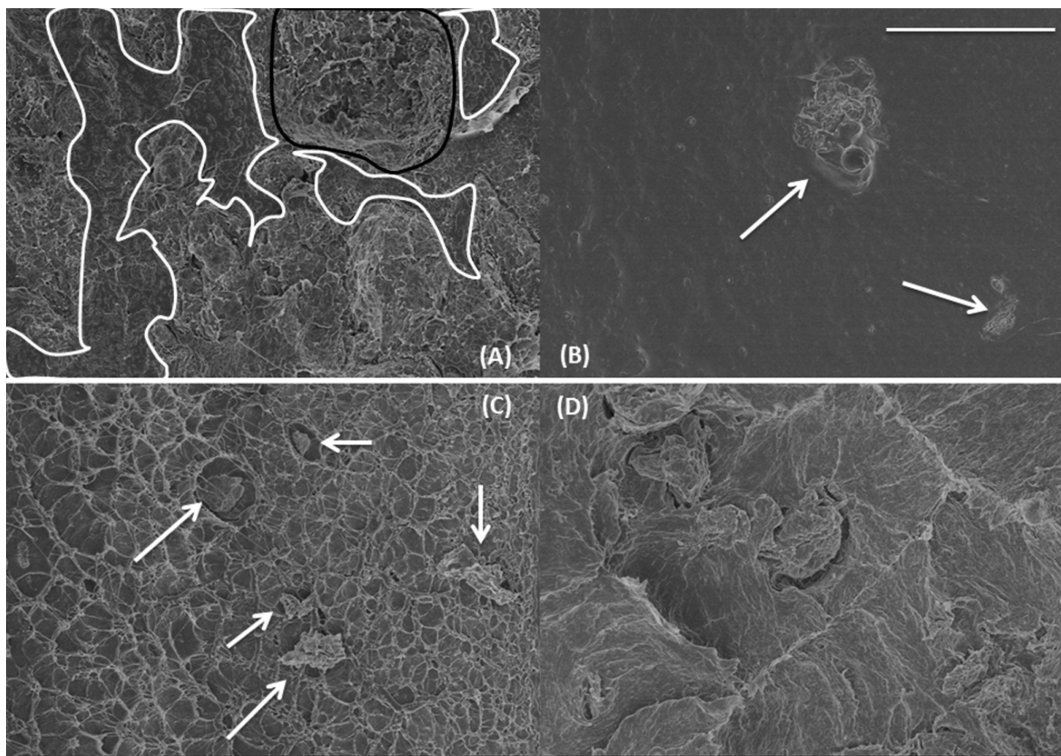


**Figure 3.** SEM images of (A) G-HDPE, (B) GTY-HDPE, (C) GAA-HDPE and (D) GTE-HDPE. The scale bar in part B applies for all samples and corresponds to 20 μm. Note: the threads that appear, especially in part C correspond to the polymer and have been created during ductile fracture due to the high elasticity of the samples.

modification with PE, the higher the compatibilization with the polymer host. In fact, this is one of the issues of the use of covalent modification of graphene, to provide functionalities capable of interacting with other groups leading to improved graphene incorporation in multicomponent systems, with the drawback of worsening the integrity of the graphene  $sp^2$  network. Considering the results in Figure 3, significant improvements in the mechanical properties as well as thermal or electrical conductivity of the GTE-HDPE sample were expected.

The Young's modulus and the elongation at break show a very interesting behavior that depends on the chemical strategy used to functionalize graphene (Table 2). In the case of the

**Table 2. Variation of the Mechanical Properties of Different HDPE Nanocomposites Studied in This Work**

sample	Young's modulus/MPa	elongation at break/%
HDPE	610 ± 30	535 ± 27
PE-OH/HDPE	369 ± 18	857 ± 53
G-HDPE	519 ± 26	218 ± 11
GAA-HDPE	477 ± 24	593 ± 30
GTE-HDPE	587 ± 29	703 ± 35
GTY-HDPE	272 ± 14	604 ± 30

former, the values for the nanocomposites were always lower than that of the raw polymer, likely to be due to the use of small amounts of short-chain PE-OH added as compatibilizer. The opposite effect could also be expected since the introduction of short-chain PE could generate some order leading to a higher degree of crystallinity that directly translates to an increase in Young's modulus. However, no changes in the crystallinity were observed (Figure S5), except in the GTE-HDPE sample. On the other hand, the effect of graphene on the variation in Young's modulus, in principle, can be attributed to some aggregation that creates points of rupture in the sample making it more fragile. Indeed the samples where graphene was not well dispersed (GTY-HDPE and GAA-HDPE) showed lower values than the raw polymer, and even lower than those of the control sample, G-HDPE. With respect to the elongation at break, a plasticizing effect is observed for all samples using click-modified graphene because of the action of the short-chain PE-OH that helps to compatibilize the HDPE matrix with the covalently modified graphene (Table 2). This can be illustrated by the value obtained for the PE-OH/HDPE sample. However, it must be pointed out that the control sample, G-HDPE shows a strong decrease in this parameter, while the GTE-HDPE sample displays the highest value of the samples containing graphene.

Those properties involving transport of species like electrons (DC-conductivity) or phonons (thermal conductivity) are expected to be very sensitive not only to the graphene dispersion in the polymer matrix but also to the quality of the  $sp^2$  network of the graphene employed. Thus, the materials prepared from chemically modified graphene were expected to be worse in these properties. Despite the fact that all the methods addressed here are based on the covalent modification of graphene, the degree of modification is higher for GTy and GAA samples, which correspondingly display lower conductivity values as mentioned earlier. After the first step of mixing with PE-OH, only the sample prepared with GTE preserved reasonable conductivity values that could allow its use as conductive filler in HDPE. Indeed only the GTE-HDPE

nanocomposite showed a measurable conductivity, of the order of  $10^{-7}$  S·cm $^{-1}$  for the composites with a graphene content of 0.74 wt %. Although this value may appear to be low, it is significant taking into account that the starting graphene source (pristine graphene) has a conductivity of approximately 20 S·cm $^{-1}$ . In addition, HDPE is insulating with conductivity values over  $10^{-14}$  S·cm $^{-1}$ , suggesting that the percolation threshold in the GTE-HDPE nanocomposites lies below 0.75 wt % of graphene. In fact the variation of the conductivity with the actual content of graphene suggests that this parameter lies between 0.37 and 0.74% graphene (see Table S2). Moreover, conductivity values in the order of 0.02 S·cm $^{-1}$  are obtained with less than 2 wt % of graphene. These results show that by means of the thiol–ene chemistry we have found a route to improve the dispersion of graphene in a HDPE matrix while obtaining at the same time reasonable conductivity values. The thiol–ene click reaction is highly efficient and high degree of modification of graphene is expected. While the reactivity of the graphene network, viewed as a hyper-conjugated alkene for this reaction, is quite low and limits the reaction yield,<sup>36</sup> this limitation becomes useful in this case because it permits a slight modification of graphene that is effective for its compatibilization with polymers, and largely preserves the integrity of the  $sp^2$  network.

Finally, the thermal conductivity of the nanocomposites has been evaluated and the results are presented in Table 3. As

**Table 3. Thermal Conductivity and the Parameters Used to Calculate It for All Samples in This Study**

sample	$X_c/\%$	$C_p/J\cdot g^{-1}\cdot K^{-1}$		$\alpha/10^7\text{ m}^2\text{ s}^{-1}$	$\kappa^a/W\cdot m^{-1}\cdot K^{-1}$
		expt	theor		
HDPE	67	1.79 ± 0.25	1.85	1.97	0.34 (0.34)
G-HDPE	66.3	1.89 ± 0.15	1.85	1.96	0.36 (0.34)
GAA-HDPE	59.9	1.85 ± 0.14	1.88	1.76	0.32 (0.31)
GTE-HDPE	60.1	1.85 ± 0.15	1.88	1.97	0.35 (0.35)
GTY-HDPE	43.0	2.13 ± 0.08	1.94	1.5	0.32 (0.28)

<sup>a</sup>The numbers in brackets correspond to the thermal conductivity calculated with the theoretical values of  $C_p$ .

shown in eq 1, the thermal conductivity depends on the thermal diffusivity, but also on the density and specific heat of the materials. The former is very difficult to be accurately measured because the samples are totally insoluble. However, since the filler content is very low we can assume that the density of the nanocomposites will not change significantly from that of the raw polymer. Therefore, we can assume this parameter to be constant at a value of  $945\text{ kg}\cdot \text{m}^{-3}$ . The specific heat ( $C_p$ ) depends on the crystallinity of the samples and has been experimentally determined using DSC. Because of the dispersion of the values obtained for distinct specimens of the same samples (Table 3) we have calculated a series of theoretical  $C_p$  values considering the degree of crystallinity<sup>61</sup> of each sample to contrast with the experimental data. The DSC crystallization thermograms show that the degree of crystallinity ( $X_c$ ) varies between samples (Figure S5), and was obtained by dividing the crystallization enthalpy of the nanocomposites obtained from the DSC curves (corrected for the amount of HDPE) by the value for 100% crystalline HDPE ( $286.2\text{ J}\cdot \text{g}^{-1}$ ).<sup>62</sup> The specific heat values were then calculated by simple addition of the contribution of the amorphous and crystalline parts according to empirical

equations.<sup>61</sup> As can be seen from Table 3, a good correlation exists between theoretical and experimental values, except for the case of the GTY-HDPE sample, whose value is a little higher than expected.

With regard to the thermal conductivity, the values for the nanocomposites do not differ much from that for the original polymer. This property behaves somewhat differently than other properties studied because while for the samples GAA-HDPE and GTY-HDPE no improvement was observed with respect to the raw polymer, G-HDPE and GTE-HDPE are slightly better. In addition, the property changes fall within experimental error and an accurate determination of the density would possibly lead to a variation in these values. The data in Table 3 shows that the results seem to be independent of the chemical modification applied to graphene. However, the quantities of graphene used in this work are too low to allow us to visualize any trends in the thermal conductivity. Indeed, recently it was proposed that substantial improvements in thermal conductivity are obtained only with relatively high amounts of graphene (10–15%).<sup>63</sup> In other words, while improvements in the thermal conductivity are harder to achieve than in electrical conductivity or mechanical properties these results were to some extent expected. In fact, within the great body of work on polymer nanocomposites only a small part deals with the study of the thermal conductivity and the majority of these are related to epoxy matrices.<sup>63–65</sup>

## CONCLUSIONS

The chemical modification of graphene by three different click chemistry approaches has been discussed along with the effects of the methodology employed on the final properties of graphene-based HDPE nanocomposites. The gradient interface methodology used for preparing the nanocomposites includes a third component, a short-chain PE-OH, whose effects on the system should not be ignored. This methodology combining the short-chain polymeric modification of graphene and the use of small amounts of free-short chain polymer represents a new and very promising strategy for engineering the graphene/polymer interface, a fundamental factor to obtain high performance lightweight graphene-based nanocomposites.

With regard to the mechanical, thermal and electrical properties it was demonstrated that the election of the appropriate chemical method to modify graphene, as well as the engineering of the interface are crucial when polymeric nanocomposites with improved final properties are required. According to the results we conclude that the best approach is that involving a thiol–ene click reaction in combination with a premixing treatment with short-chain PE-OH. The chemical reaction employed is a well-known and highly efficient thiol–ene click reaction that, in principle, should give a higher degree of modification of graphene; however, the reactivity of the graphene network is quite low, limiting the polymer grafting density. In this case this limitation is useful because permits a “friendly” modification of graphene that is efficient for its compatibilization with polymers but largely preserves the integrity of the sp<sup>2</sup> network. In addition the reaction is directly conducted on the graphene surface without the need to provide it with other functionalities that inevitably lead to damage of the graphene sp<sup>2</sup> network and a worsening of its properties.

Although only addressed here in the case of PE, these chemical routes constitute general tools that are wide in scope and can, in principle, be extended to other polymer families.

## ASSOCIATED CONTENT

### Supporting Information

Additional experimental details on the PE-OH functionalization, Raman spectra of click products, characterization of nanocomposites, and information used to calculate the theoretical specific heat of all nanocomposites. This material is available free of charge via the Internet at <http://pubs.acs.org>.

## AUTHOR INFORMATION

### Corresponding Author

(H.J.S.) Fax: +34915644853. Telephone: +34-912587432. E-mail: horacio@ictp.csic.es.

### Notes

The authors declare no competing financial interest.

## ACKNOWLEDGMENTS

This work was funded by the Spanish Ministry of Economy and Competitiveness (MINECO) projects MAT 2009-09335 and MAT 2010-21070-01. H.J.S. thanks the MINECO for a Ramon y Cajal Senior Research Fellowship. M.C. is indebted to the Consejo Superior de Investigaciones Científicas (CSIC) for a JAE predoc fellowship. The authors also wish to thank I. Muñoz of the ICTP Characterization Service for her assistance in recording the Raman data. The authors wish to thank the reviewers of this manuscript for helpful comments.

## REFERENCES

- (1) Kuila, T.; Bose, S.; Mishra, A. K.; Khanra, P.; Kim, N. H.; Lee, J. H. *Prog. Mater. Sci.* **2012**, *57* (7), 1061–1105.
- (2) Kuilla, T.; Bhadra, S.; Yao, D.; Kim, N. H.; Bose, S.; Lee, J. H. *Prog. Polym. Sci.* **2010**, *35* (11), 1350–1375.
- (3) RamanathanT; Abdala, A. A.; StankovichS; Dikin, D. A.; Herrera Alonso, M.; Piner, R. D.; Adamson, D. H.; Schniepp, H. C.; Chen, X.; Ruoff, R. S.; Nguyen, S. T.; Aksay, I. A.; Prud'Homme, R. K.; Brinson, L. C. *Nat. Nano* **2008**, *3* (6), 327–331.
- (4) Salavagione, H. J.; Martínez, G.; Ellis, G. *Macromol. Rapid Commun.* **2011**, *32* (22), 1771–1789.
- (5) Zaman, I.; Kuan, H.-C.; Meng, Q.; Michelmore, A.; Kawashima, N.; Pitt, T.; Zhang, L.; Gouda, S.; Luong, L.; Ma, J. *Adv. Funct. Mater.* **2012**, *22* (13), 2735–2743.
- (6) Ye, Y.-S.; Chen, Y.-N.; Wang, J.-S.; Rick, J.; Huang, Y.-J.; Chang, F.-C.; Hwang, B.-J. *Chem. Mater.* **2012**, *24* (15), 2987–2997.
- (7) Salavagione, H. J.; Martinez, G.; Ellis, G. Graphene-Based Polymer Nanocomposites. In *Physics and Applications of Graphene—Experiments*; Mikhailov, S., Ed.; Intech: Rijeka, Croatia, 2011; pp 169–192.
- (8) Salavagione, H. J. Innovative Strategies to Incorporate Graphene in Polymer Matrices: Advantages and Drawbacks from an Applications Viewpoint in Innovative Graphene Technologies: Developments & Characterisation. In *Innovative graphene technologies: developments and characterisation*; Tiwari, A., Ed.; Smithers-Rapra: Shawbury, U.K., 2013; Vol. 1, pp 177–221.
- (9) Verdejo, R.; Bernal, M. M.; Romasanta, L. J.; Lopez-Manchado, M. A. *J. Mater. Chem.* **2011**, *21* (10), 3301–3310.
- (10) Dreyer, D. R.; Park, S.; Bielawski, C. W.; Ruoff, R. S. *Chem. Soc. Rev.* **2010**, *39* (1), 228–240.
- (11) Salavagione, H. J.; Martinez, G.; Marco, C. *J. Mater. Chem.* **2012**, *22* (14), 7020–7027.
- (12) Song, M.; Cai, D., Chapter 1 Graphene Functionalization: A Review. In *Polymer-Graphene Nanocomposites*; The Royal Society of Chemistry: London, 2012; pp 1–52.
- (13) Englert, J. M.; Dotzer, C.; Yang, G.; Schmid, M.; Papp, C.; Gottfried, J. M.; Steinrück, H.-P.; Spiecker, E.; Hauke, F.; Hirsch, A. *Nature Chem.* **2011**, *3* (4), 279–286.

- (14) Georgakilas, V.; Otyepka, M.; Bourlinos, A. B.; Chandra, V.; Kim, N.; Kemp, K. C.; Hobza, P.; Zboril, R.; Kim, K. S. *Chem. Rev.* **2012**, *112* (11), 6156–6214.
- (15) Dai, L. *Acc. Chem. Res.* **2012**, *46* (1), 31–42.
- (16) Park, J.; Yan, M. *Acc. Chem. Res.* **2012**, *46* (1), 181–189.
- (17) Zhang, H.; Bekyarova, E.; Huang, J.-W.; Zhao, Z.; Bao, W.; Wang, F.; Haddon, R. C.; Lau, C. N. *Nano Lett.* **2011**, *11* (10), 4047–4051.
- (18) Sarkar, S.; Bekyarova, E.; Haddon, R. C. *Acc. Chem. Res.* **2012**, *45* (4), 673–682.
- (19) Fang, M.; Wang, K.; Lu, H.; Yang, Y.; Nutt, S. *J. Mater. Chem.* **2010**, *20* (10), 1982–1992.
- (20) Fang, M.; Wang, K.; Lu, H.; Yang, Y.; Nutt, S. *J. Mater. Chem.* **2009**, *19* (38), 7098–7105.
- (21) Salavagione, H. J.; Gómez, M. A.; Martínez, G. *Macromolecules* **2009**, *42* (17), 6331–6334.
- (22) He, H.; Gao, C. *Chem. Mater.* **2010**, *22* (17), 5054–5064.
- (23) Lock, E. H.; Baraket, M.; Laskoski, M.; Mulvaney, S. P.; Lee, W. K.; Sheehan, P. E.; Hines, D. R.; Robinson, J. T.; Tosado, J.; Fuhrer, M. S.; Hernández, S. C.; Walton, S. G. *Nano Lett.* **2011**, *12* (1), 102–107.
- (24) Jin, Z.; McNicholas, T. P.; Shih, C.-J.; Wang, Q. H.; Paulus, G. L. C.; Hilmer, A. J.; Shimizu, S.; Strano, M. S. *Chem. Mater.* **2011**, *23* (14), 3362–3370.
- (25) Pan, Y.; Bao, H.; Sahoo, N. G.; Wu, T.; Li, L. *Adv. Funct. Mater.* **2011**, *21* (14), 2754–2763.
- (26) Sumerlin, B. S.; Vogt, A. P. *Macromolecules* **2009**, *43* (1), 1–13.
- (27) Clave, G.; Campidelli, S. *Chemical Science* **2011**, *2* (10), 1887–1896.
- (28) Segura, J. L.; Salavagione, H. J. *Curr. Org. Chem.* **2013**, *17* (15), 1680–1693.
- (29) Castelaín, M.; Martínez, G.; Merino, P.; Martín-Gago, J. Á.; Segura, J. L.; Ellis, G.; Salavagione, H. J. *Chem.—Eur. J.* **2012**, *18* (16), 4965–4973.
- (30) Cao, Y.; Lai, Z.; Feng, J.; Wu, P. *J. Mater. Chem.* **2011**, *21* (25), 9271–9278.
- (31) Sun, S.; Cao, Y.; Feng, J.; Wu, P. *J. Mater. Chem.* **2010**, *20* (27), S605–S607.
- (32) Jing, Y.; Tang, H.; Yu, G.; Wu, P. *Polym. Chem.* **2013**, *4* (8), 2598–2607.
- (33) Rostovtsev, V. V.; Green, L. G.; Fokin, V. V.; Sharpless, K. B. *Angew. Chem., Int. Ed.* **2002**, *41* (14), 2596–2599.
- (34) Tornøe, C. W.; Christensen, C.; Meldal, M. J. *Org. Chem.* **2002**, *67* (9), 3057–3064.
- (35) Hoyle, C. E.; Lowe, A. B.; Bowman, C. N. *Chem. Soc. Rev.* **2010**, *39* (4), 1355–1387.
- (36) Lowe, A. B. *Polym. Chem.* **2010**, *1* (1), 17–36.
- (37) Cramer, N.; Scott, J. P.; Bowman, C. *Macromolecules* **2002**, *35* (14), 5361–5365.
- (38) Campos, L.; Killopp, K.; Sakai, R.; Damiron, D.; Drockenmuller, E.; Messmore, B.; Hawker, C. *Macromolecules* **2008**, *41* (19), 7063–7070.
- (39) Espeel, P.; Goethals, F.; Du Prez, F. E. *J. Am. Chem. Soc.* **2011**, *133* (6), 1678–1681.
- (40) Hoyle, C. E.; Bowman, C. N. *Angew. Chem., Int. Ed.* **2010**, *49* (9), 1540–1573.
- (41) Fu, R.; Fu, G.-D. *Polym. Chem.* **2011**, *2* (3), 465–475.
- (42) Ye, S.; Cramer, N. B.; Smith, I. R.; Voigt, K. R.; Bowman, C. N. *Macromolecules* **2011**, *44* (23), 9084–9090.
- (43) Fairbanks, B. D.; Scott, T. F.; Kloxin, C. J.; Anseth, K. S.; Bowman, C. N. *Macromolecules* **2008**, *42* (1), 211–217.
- (44) Marvel, C. S.; Aldrich, P. H. *J. Am. Chem. Soc.* **1950**, *72* (5), 1978–1981.
- (45) Fairbanks, B. D.; Sims, E. A.; Anseth, K. S.; Bowman, C. N. *Macromolecules* **2010**, *43* (9), 4113–4119.
- (46) Marvel, C. S.; Cripps, H. N. *J. Polym. Sci.* **1952**, *8* (3), 313–320.
- (47) Marvel, C. S.; Markhart, A. H. *J. Polym. Sci.* **1951**, *6* (6), 711–716.
- (48) Nuyken, O.; Reuschel, G.; Siebzehnrübl, F. *Makromol. Chem. Macromol. Symp.* **1989**, *26* (1), 313–331.
- (49) Nuyken, O.; Hofinger, M. *Polym. Bull.* **1984**, *11* (2), 165–170.
- (50) Yang, H.; Liu, M.-X.; Yao, Y.-W.; Tao, P.-Y.; Lin, B.-P.; Keller, P.; Zhang, X.-Q.; Sun, Y.; Guo, L.-X. *Macromolecules* **2013**, *46* (9), 3406–3416.
- (51) Lu, D.; Jia, Z.; Monteiro, M. *Polym. Chem.* **2013**, *4* (6), 2080–2089.
- (52) Korthals, B.; Morant Minana, M.; Schmid, M.; Mecking, S.; Morant Miñana, M. *Macromolecules* **2010**, *43* (19), 8071–8078.
- (53) Castelaín, M.; Martínez, G.; Ellis, G.; Salavagione, H. J. *Chem. Commun.* **2013**, *49* (79), 8967–8968.
- (54) Castelaín, M.; Shuttleworth, P. S.; Marco, C.; Ellis, G.; Salavagione, H. J. *Phys. Chem. Chem. Phys.* **2013**, *15* (39), 16806–16811.
- (55) Niyogi, S.; Bekyarova, E.; Itkis, M. E.; Zhang, H.; Shepperd, K.; Hicks, J.; Sprinkle, M.; Berger, C.; Lau, C. N.; deHeer, W. A.; Conrad, E. H.; Haddon, R. C. *Nano Lett.* **2010**, *10* (10), 4061–4066.
- (56) Dresselhaus, M. S.; Jorio, A.; Hofmann, M.; Dresselhaus, G.; Saito, R. *Nano Lett.* **2010**, *10* (3), 751–758.
- (57) Bian, S.; Scott, A. M.; Cao, Y.; Liang, Y.; Osuna, S.; Houk, K. N.; Braunschweig, A. B. *J. Am. Chem. Soc.* **2013**, *135* (25), 9240–9243.
- (58) Ferrari, A. C. *Solid State Commun.* **2007**, *143* (1–2), 47–57.
- (59) Martins Ferreira, E. H.; Moutinho, M. V. O.; Stavale, F.; Lucchese, M. M.; Capaz, R. B.; Achete, C. A.; Jorio, A. *Phys. Rev. B* **2010**, *82* (12), 125429.
- (60) Jorio, A.; Martins-Ferreira, E. H.; Cançado, I. G.; Achete, C. A.; Capaz, R. B. Measuring disorder in graphene with Raman spectroscopy. In *Physics and applications of graphene—Experiments*; Mikhailov, S., Ed.; Intech: Rijeka, Croatia, 2011; pp 439–454.
- (61) Wunderlich, B. *J. Chem. Phys.* **1962**, *37* (6), 1203–1207.
- (62) Wunderlich, B.; Cormier, C. M. *J. Polym. Sci., Part A-2: Polym. Phys.* **1967**, *5* (SPA2), 987–988.
- (63) Shahil, K. M. F.; Balandin, A. A. *Nano Lett.* **2012**, *12* (2), 861–867.
- (64) Song, S. H.; Park, K. H.; Kim, B. H.; Choi, Y. W.; Jun, G. H.; Lee, D. J.; Kong, B.-S.; Paik, K.-W.; Jeon, S. *Adv. Mater.* **2013**, *25* (5), 732–737.
- (65) Wu, H.; Drzal, L. T. *Carbon* **2012**, *50* (3), 1135–1145.